INITIAL TESTING OF A TWO-DIMENSIONAL COMPUTER CODE FOR MICROWAVE-INDUCED SURFACE BREAKDOWN IN AIR*

D.J. Mayhall and J.H. Yee
Lawrence Livermore National Laboratory
University of California
P.O. Box 808, Mail Code L-156
Livermore, CA 94551

Abstract

A two-dimensional, electromagnetic, electron fluid computer code for microwave-induced surface breakdown in air is developed. This code is based on finite difference approximations to Maxwell's curl equations for TM_{om} modes in cylindrical waveguides and electron conservation equations for continuity, momentum, and energy. An implicit, block-iterative, optionally stiff, variable step integrator solves the global set of equations. A 2.856 GHz, 1 MV/m amplitude, radial electric field pulse in a highly dispersive waveguide impinges on two different model field emission structures with the same emission threshold (0.2 MV/m) and rate (10^{11}/(m^3–s)). One structure is a perfectly conducting flat end plate; the other is a perfectly conducting axial stub of 0.413 cm radius by 1.69 cm length, centered on a flat end plate. Pressures vary from 50–800 torr. In both cases, peak electric fields occur where expected, initial electron generation is from field emission, and later generation is from avalanching in air. The location of peak generation is at the field maxima. The amount of late time density varies qualitatively with pressure as theoretically expected.

Introduction

Subjects of great importance in the design and operation of high-voltage electrical equipment are electron emission and surface flashover. As a step toward further understanding of these phenomena in gas-insulated, high-power microwave structures, we have developed a two-dimensional, electromagnetic, electron fluid computer code in an r-z cylindrical coordinate system with azimuthal symmetry. This code is intended for simulation of microwave-induced surface breakdown in air-insulated cylindrical waveguide structures. Other insulating gases can be considered by the specification of collision frequencies for ionization and momentum and energy transfer to neutral molecules. Although the initial computational tests involve field emission from purely metallic structures, the code can be adapted for emission from dielectrics.

Governing Equations

Maxwell's curl equations for the TM_{om} mode electromagnetic components in a nonmagnetic, gaseous medium in a cylindrical symmetric coordinate system in MKS units are

$$\frac{\partial H_\phi}{\partial t} = \mu_o^{-1}\left(\frac{\partial E_z}{\partial r} - \frac{\partial E_r}{\partial z}\right), \tag{1}$$

$$\frac{\partial E_r}{\partial t} = -\varepsilon_o^{-1}\left(\frac{\partial H_\phi}{\partial z} + nev_r\right), \tag{2}$$

$$\frac{\partial E_z}{\partial t} = \varepsilon_o^{-1}\left(\frac{1}{r}\frac{\partial(rH_\phi)}{\partial z} - nev_z\right), \tag{3}$$

where H_ϕ is the azimuthal magnetic field, E_r and E_z are the radial and axial electric fields, μ_o and ε_o are the free space permeability and permittivity, n is the electron density , e is the electron charge (-1.6×10^{-19} C), and v_r and v_z are the radial and axial electron velocities.

One set of approximate electron fluid conservation equations is

$$\frac{\partial n}{\partial t} = nv_i - \frac{1}{r}\frac{\partial}{\partial r}(rnv_r) - \frac{\partial(nv_z)}{\partial z} + g, \tag{4}$$

$$\frac{\partial v_r}{\partial t} = em^{-1}E_r - v_r\left(v_i + v_m + gn^{-1}\right), \tag{5}$$

$$\frac{\partial v_z}{\partial t} = em^{-1}E_z - v_z\left(v_i + v_m + gn^{-1}\right), \tag{6}$$

$$\frac{\partial U}{\partial t} = e\left(v_rE_r + v_zE_z\right) + v_uU_o - \varepsilon_iv_i - U\left(v_i + v_u + gn^{-1}\right), \tag{7}$$

where v_i is the ionization collision frequency, g is the volumetric electron emission rate, m is the electron mass, v_m is the electron-neutral molecule momentum transfer collision frequency, U is the electron kinetic energy, v_u is the electron-neutral energy transfer collision frequency, U_o is the average neutral energy, and ε_i is the average neutral ionization potential. For air, U_o is 0.025 eV and ε_i is 14 eV. Among the terms neglected are magnetic forces, atomic and molecular electron losses, emitted electron momentum and energy, convected energy and momentum, pressure gradients, and heat flows. A Maxwellian velocity distribution is assumed. The electron emission rate is zero except in computational cells next to emitting surfaces, where it may be non-zero under prescribed conditions. The collision frequencies used for air are those previously used for one-dimensional microwave propagation in the atmosphere [1,2] and two-dimensional propagation in waveguides [3,4].

Computational Geometry

Figure 1 shows the geometry for the computer code. The radial coordinate extends from 0 to r_m; the axial coordinate extends from 0 to z_m. Perfectly conducting boundary conditions, for which the transverse
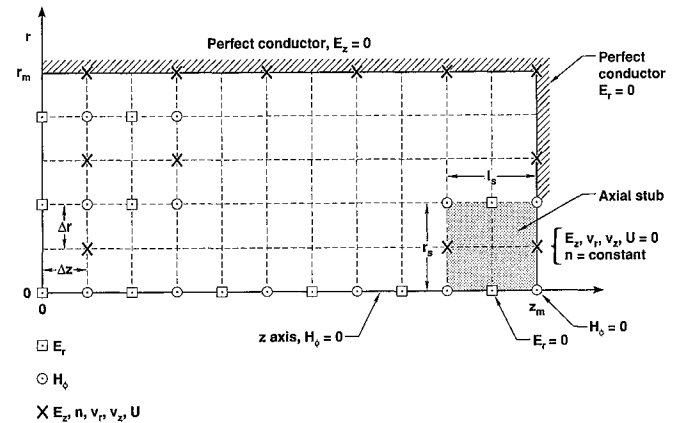

Figure 1. Computational geometry.

		Form Approved
Report Documentation Page		OMB No. 0704-0188

1. REPORT DATE **JUN 1991**	2. REPORT TYPE **N/A**	3. DATES COVERED **-**

4. TITLE AND SUBTITLE	5a. CONTRACT NUMBER
Initial Testing Of A Two-Dimensional Computer Code For Microwave-Induced Surface Breakdown In Air	5b. GRANT NUMBER
	5c. PROGRAM ELEMENT NUMBER
6. AUTHOR(S)	5d. PROJECT NUMBER
	5e. TASK NUMBER
	5f. WORK UNIT NUMBER

7. PERFORMING ORGANIZATION NAME(S) AND ADDRESS(ES) **Lawrence Livermore National Laboratory University of California P.O. Box 808, Mail Code L-156 Livermore, CA 94551**	8. PERFORMING ORGANIZATION REPORT NUMBER
9. SPONSORING/MONITORING AGENCY NAME(S) AND ADDRESS(ES)	10. SPONSOR/MONITOR'S ACRONYM(S)
	11. SPONSOR/MONITOR'S REPORT NUMBER(S)

12. DISTRIBUTION/AVAILABILITY STATEMENT
Approved for public release, distribution unlimited

13. SUPPLEMENTARY NOTES
See also ADM002371. 2013 IEEE Pulsed Power Conference, Digest of Technical Papers 1976-2013, and Abstracts of the 2013 IEEE International Conference on Plasma Science. Held in San Francisco, CA on 16-21 June 2013. U.S. Government or Federal Purpose Rights License.

14. ABSTRACT

A two-dimensional, electromagnetic, electron fluid computer code for microwave-induced surface breakdown in air is developed. This code is based on finite difference approximations to Maxwell's curl equations for â¢am modes in cylindrical waveguides and electron conservation equations for continuity, momentum, and energy. An implicit, blockiterative, optionally stiff, variable step integrator solves the global set of equations. A 2.856 GHz, 1 MV/m amplitude, radial electric field pulse in a highly dispersive waveguide impinges on two different model field emission structures with the same emission threshold (0.2 MV /m) and rate (1011 /(m3-s)). One structure is a perfectly conducting flat end plate; the other is a perfectly conducting axial stub of 0.413 em radius by 1.69 em length, centered on a flat end plate. Pressures vary from 50-800 torr. In both cases, peak electric fields occur where expected, initial electron generation is from field emission, and later generation is from avalanching in air. The location of peak generation is at the field maxima. The amount of late time density varies qualitatively with pressure as theoretically expected.

15. SUBJECT TERMS

16. SECURITY CLASSIFICATION OF:			17. LIMITATION OF ABSTRACT	18. NUMBER OF PAGES	19a. NAME OF RESPONSIBLE PERSON
a. REPORT **unclassified**	b. ABSTRACT **unclassified**	c. THIS PAGE **unclassified**	**SAR**	**5**	

electric field vanishes, are imposed at the surfaces r_m and z_m. The computational space thus defined represents the interior of a cylindrical waveguide or can with the left end open. The center line of the can is the z axis. A cylindrical, axially centered, perfectly conducting stub of radius r_s and length l_s may join the flat end plate at the right. Such a stub is shown in Fig. 1. Other concentric structures at the end plate are also possible.

A regular mesh of uniform axial spacing Δz and radial spacing Δr partitions the computational space. The seven solution variables—H_ϕ, E_r, E_z, n, v_r, v_z, and U—are located to create a staggered grid. Because of its convenience for central differencing of Maxwell's curl equations, this type of grid appears extensively in explicit, finite difference, electromagnetic scattering codes, such that of Yee [5]. As shown by the symbols in Fig. 1, H_ϕ occurs at grid points with even axial indices and odd radial indices. E_r occurs at grid points with both odd axial and radial indices. E_z exists at points with both even axial and radial indices. The four electron fluid quantities occur at the same points as E_z.

Additional Boundary Conditions

For the considered test cases, an input radial electric field of 1 MV/m amplitude for the TM_{01} mode is specified as a time function along the left grid boundary. No other condition is imposed there. Since the left boundary has no radiation condition, a spurious reflection occurs there when a reflected wave from the right side impinges on this boundary. The calculation near the left boundary is thus only good for ~2 τ, where τ is the wave transit time from the left boundary to the right. This defect can be easily remedied. The upper boundary is presently assumed to emit no electrons. The right boundary is perfectly conducting. When an axial stub is included, the condition that all variables, except the electron density, vanish is imposed within the stub. Within the stub, the electron density is a small number, typically $10^{-3}m^{-3}$, constant in time. The face and the lateral surface of the stub are perfectly conducting. The face of the stub and the end plate emit electrons at the constant volumetric rate g when E_z is positive and equal to or greater than some constant threshold value E_{th}. Due to azimuthal symmetry, H_ϕ is zero along the bottom boundary.

Numerical Solution by Finite Differences

In the mesh interior, central finite differences replace the spatial gradients in Eqs. (1)–(4). At the boundaries, one-sided differences are used. The result of this discretization is a global set of ordinary differential equations in time. The implicit, block-iterative, optionally stiff, variable step software package GEARBI then integrates the system in time [6].

GEARBI has several attractive features for electromagnetic problems involving time scale changes due to avalanche ionization or electron emission. The variable integration step allows steps somewhat greater than the Courant stability limit when wave propagation is the only time-varying process. When ionization becomes significant, the solver can take smaller steps of the order of v_i^{-1}. The code can thus use a much smaller amount of computation time than a fixed-step code set to resolve solution variation for a high ionization rate. The stiff option allows larger time steps for stiff problems, that is, with disparate time scales of varying amplitude, than can a code without this capability. The block-iterative solution method reduces the memory requirement for a given grid size as compared to a conventional direct solver.

Test Problems

Two test problems involving field emission from perfect conductors are considered. The emission threshold is 0.2 MV/m. The emission rate is 10^{11} electrons/(m^3–s), except as noted. These values do not represent any real material surface, but serve as a starting point for testing the code. In each problem, a 1 ns-long radial electric field pulse at 2.856 GHz enters the left, open end of a cylindrical can of inner radius 4.445 cm. An end plate terminates the can at 41.5 cm to the right. This geometry was chosen for simulation of planned experiments.

In one problem, the vertical end plate is absolutely flat. In the other, a cylindrical, perfectly conducting, inwardly protruding, axially centered, electric field enhancing stub joins the end plate. This stub is 1.69 cm long

and 0.413 cm in radius. The grid for each problem has 200 points in the axial direction and 44 in the radial direction.

Results for the Flat End Plate

As the input pulse propagates from the open end toward the end plate, it experiences strong dispersion as a result of the chosen radius and frequency. Figure 2a shows the radial electric field at 1.45 ns, just before the leading edge of the pulse strikes the end plate. Figure 2b shows the
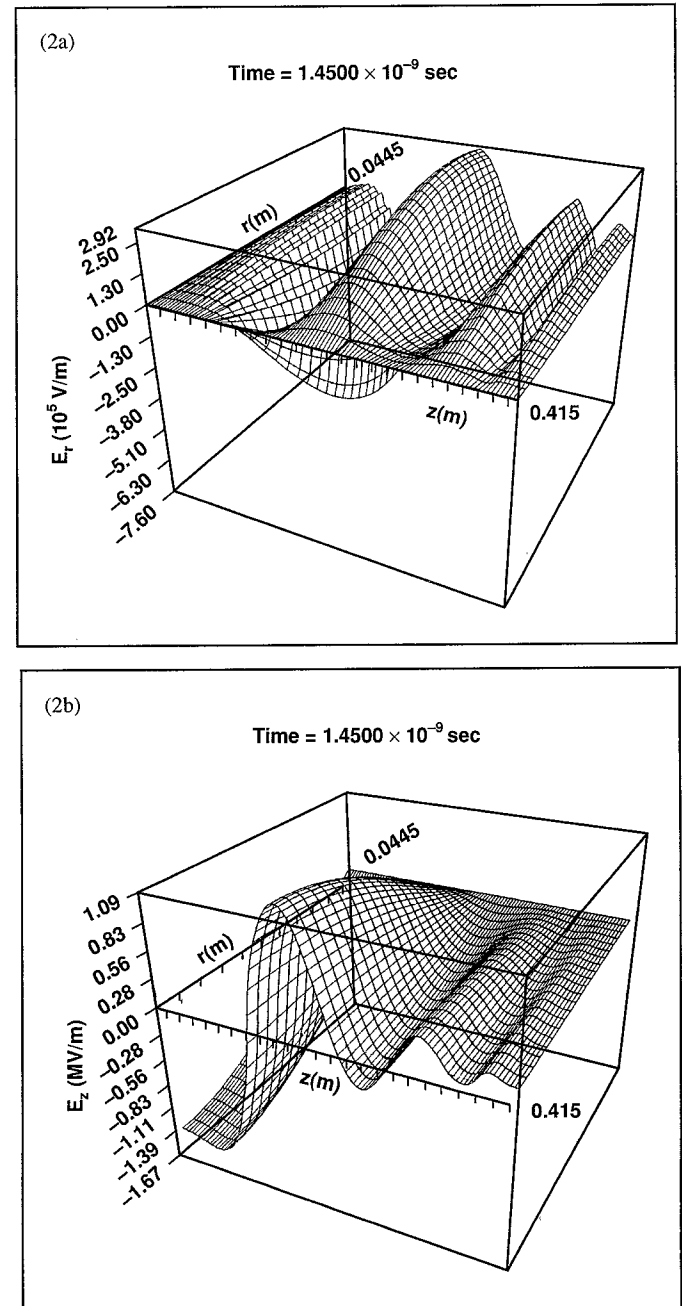
Figure 2. Microwave electric fields just befor hitting the flat end plate: (a) radial field; (b) axial field.

axial electric field at the same time. Instead of 2.9 cycles of a 1 MV/m modulated square pulse filling about 72% of the axial space, somewhat more than 3 cycles of a 760 kV/m, dispersed pulse fills the entire axial space. The high-frequency components precede the lower frequencies to the end plate.

As the wave initially impinges on the plate, an axial electrical field positive half cycle builds up. When this axial field reaches the emission threshold, emission begins, causing the electron density abruptly to

370

(3a)

Time = 1.7000 × 10⁻⁹ sec

Time = 2.3500 × 10⁻⁹ sec

Figure 4. Electron density at 2.35 ns at the flat end plate.
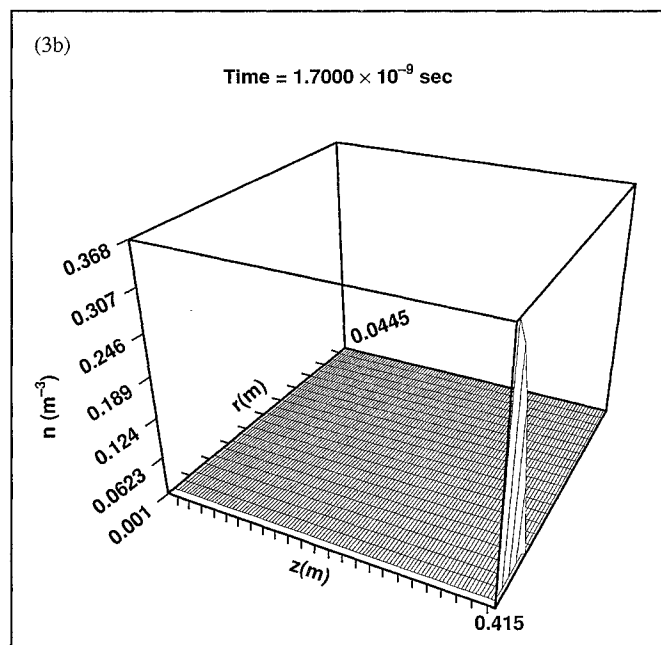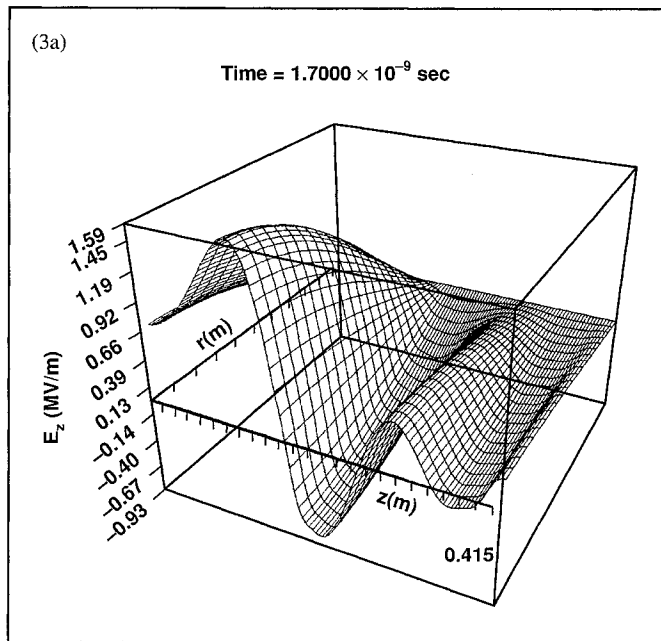

(3b)

Time = 1.7000 × 10⁻⁹ sec

Figure 3. Appearance of electron density due to field emission at the flat end plate: (a) axial field; (b) electron density.

exceed the background level of $10^{-3}m^{-3}$. At an 0.05 ns output interval and 300 torr, the first electron density enhancement appears at 1.70 ns into the calculation. Figure 3 shows the axial field and the density at this time. Since E_z first reaches the threshold at one radial grid space above the z axis, the peak electron density occurs there. During the initial positive E_z half cycle, the electron density at the end plate expands radially outward from 0.10³ cm to 1.55 cm. A maximum of 4.1948 m⁻³ occurs near the axis.

During the next 0.20 ns, E_z drops below the threshold, experiences a negative half cycle, and then returns to threshold. During this interval when no emission occurs, the peak density drops to 4.1899 m⁻³. Since no other electron losses are allowed, this is probably evidence of convective loss. Within the second positive half cycle of E_z, the peak density increases to 13.453 m⁻³, and the radial profile expansion reaches 2.79 cm. This expansion, as shown in Fig. 4, occurs primarily because the radial span of E_z at the end plate above the threshold increases with time.

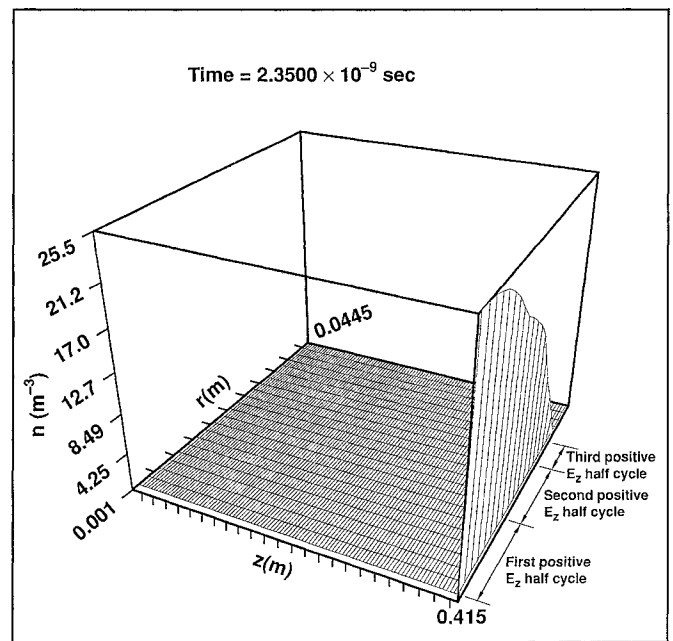In the second negative half cycle of E_z, the peak density decreases to

13.434 m⁻³. During the third positive half cycle, the density profile reaches 3.41 cm radially, and the peak value achieves 25.472 m⁻³. The electron density at the end plate at 2.35 ns, just after the third positive E_z half cycle, is shown in Fig. 4. The three radial modulations in the profile outward from the axis are due to additional emission during the three positive half cycles of E_z. The extent of the density from each half cycle is shown in the figure. After the third positive half cycle, the radial density expansion proceeds at a slower rate. The final outer radius of 4.03 cm occurs at 2.90 ns. Thereafter the peak density increases, and the profile suffers slight changes in shape, but the outer radius does not vary.

From displays like Fig. 2a, the one-way, initial transit time of E_r down the axis is $\tau \sim 1.50$ ns. The first reflection from the end plate should reach the left boundary at $2\tau \sim 3.0$ ns. A contaminating, nonphysical return reflection from the unterminated left boundary should reach the end plate at ~4.5 ns. Thus, the calculation at the end plate should be good until around 4.5 ns.

After 2.7 ns, the peak density also increases throughout negative half cycles of E_z when the peak E_z is of the order of 1.5 MV/m and the half cycles are longer as a result of the dispersive delay of the lower-frequency pulse components. This density increase must be due to avalanche ionization in the low-pressure air near the axis around the negative peaks of E_z.

These calculations have been repeated from 50–800 torr. Table 1 gives the peak electron density at four times for ten pressures. Those values denoted with an asterisk occurred near the axis at input of the can. At 100 and 50 torr, avalanche ionization in the air becomes increasingly significant.

Table 1. Peak electron densities for the flat end plate.

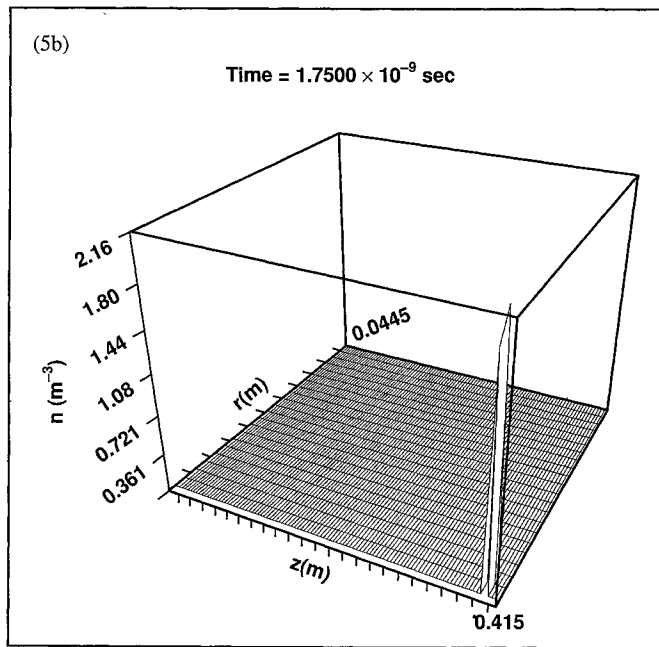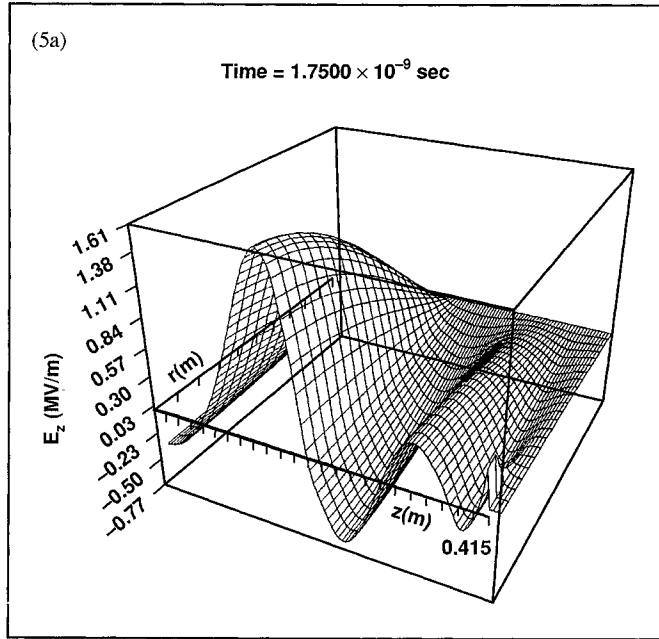| Pressure (torr)	Peak Electron Density (m⁻³)			
	1.70 ns	1.75 ns	2.35 ns	3.65 ns
50	*9.0232 × 10³	*9.4609 × 10³	*5.5600 × 10⁴	*5.1500 × 10⁵
100	*0.59506	4.2183	25.981	1.3467 × 10³
200	0.36778	4.1558	25.543	169.89
300	0.36765	4.1948	25.472	108.05
400	0.36676	4.1796	25.473	97.713
500	0.36780	4.1348	25.348	90.402
600	0.36690	4.1463	25.431	88.876
700	0.36739	4.1945	25.504	88.301
760	0.36733	4.1789	25.552	88.125
800	0.36767	4.1993	25.520	87.649

371

Figure 5. *Appearance of electron density due to field emission at the axial stub: (a) Axial field; (b) electron density.*

Table 2. Peak Electron Densities for the Axial Stub

Pressure (torr)	Peak Electron Density (m^{-3})		
	1.75 ns	2.35 ns	3.65 ns
50	*9.3457×10^3	*5.4777×10^4	>4.1303×10^{19a}
100	2.1630	196.52	1.3689×10^{17}
200	2.1631	54.934	2.5735×10^8
300	2.1633	40.510	1.9417×10^5
400	2.1631	36.168	7.7705×10^3
500	2.1631	34.649	1.4557×10^3
600	2.1633	34.195	555.20
700	2.1639	33.652	309.36
760	2.1636	33.670	242.85
800	2.1634	33.774	213.03

Table 3. Peak Electron Densities for the Axial Stub Versus Emission Rate at 700 torr

Emission rate (m^3–$s)^{-1}$	Peak Electron Density (m^{-3})		
	1.75 ns	2.35 ns	3.65 ns
10^{11}	2.1639	33.652	309.36
10^{12}	21.630	339.77	3.1067×10^3
10^{13}	216.28	3.3737×10^3	3.0928×10^4

density at the stub face greatly dwarfs that along the end plate.

Calculations with the stub have been done from 50–800 torr. Table 2 gives the peak electron density versus pressure for three times. Once again values marked with an asterisk indicate values at the left side of the grid near the z axis. The value in the 3.65 ns column marked with the "a" occurred at 3.27 ns. Beyond this time, the code slowed down to very tiny time steps and could not make any progress in a practical interval of computation time.

At 1.75 ns, shortly after emission begins, there is practically no difference in the peak electron density at the stub face from 100–800 torr. At 2.35 ns, there is very little difference in the peak density from 300–800 torr. However by 3.65 ns, the difference at various pressures amounts to many orders of magnitude, which is indicative of electron generation by avalanche ionization. As the pressure decreases, the threshold electric field for breakdown or strong avalanching decreases, and the ionization rate increases. Decrease of the pressure corresponds to movement down the right side of the Paschen curve toward the minimum breakdown threshold at several torr. The avalanche-generated density is expected to vary roughly exponentially with the product of the average ionization rate and the time interval. The ionization rate increases with decreasing pressure. Therefore the density at later times should be much greater at lower pressures than at higher pressures for electric fields at and beyond the breakdown threshold.

Table 3 shows the peak electron density for 700 torr at three times during calculations with an increase in the constant emission rate. The density at each time scales almost exactly with the emission rate. This behavior indicates that avalanche ionization is not important for the calculational parameters at 700 torr. This is not the case at sufficiently lower pressure.

Comparison of Tables 1 and 2 shows that at late times avalanche ionization becomes important for the flat end plate at pressures below 100–200 torr. Below 400–500 torr, ionization becomes increasingly important for the stub. This is because the electric field enhancement of the stub generates strong fields, which stay above the emission threshold for longer time intervals than for the flat end plate.

Results for the Axial Stub

For this problem at 300 torr and an output interval of 0.05 ns, the first appearance of significant electron density is at 1.75 ns at the stub face. The axial electric field at 1.75 ns is shown in Fig. 5a, and the density is shown in Fig. 5b. The electron density is greatest near the outer edge of the stub, where the enhancement of E_z is greatest. The electron density at the stub face increases monotonically in time. This indicates that avalanche ionization from field enhancement at the stub occurs during negative half cycles of E_z.

Electron density first appears at the end plate at 1.95 ns, which is during the second positive half cycle of E_z. This density extends from 1.14 to 2.58 cm in a radial profile similar to a positive half cosine.

Because of the stronger axial field at the face of the stub and its longer time above the threshold, the electron density increases more rapidly at the stub face than along the end plate. At the later times, the

Conclusions

Two initial test cases of a two-dimensional, cylindrically symmetric, electron fluid computer code for microwave-induced surface breakdown in air with model electron field emission show that the code behaves qualitatively as expected over a range of decreasing pressure. Many other aspects of the code remain to be tested, including, most importantly, careful validation against experimental data for a number of structural arrangements. Thus far, the code offers good promise for problems of microwave-induced surface breakdown involving field emission from materials with gas insulation.

References

[1] J.H. Yee, R.A. Alvarez, D.J. Mayhall, D.P. Byrne, and J. DeGroot, "Theory of Short, Intense Electromagnetic-Pulse Propagation Through the Atmosphere," Phys. Fluids, vol. 29, pp. 1238-1244, April 1986.

[2] G.E. Sieger, D.J. Mayhall, and J.H. Yee, Laser Interaction And Related Plasma Phenomena, vol. 8, H. Hora and G. Miley, Eds., New York: Plenum Press, 1988, pp. 139–148.

[3] D.J. Mayhall, J.H. Yee, R.A. Alvarez, and D.P. Byrne, Laser Interaction And Related Plasma Phenomena, vol. 8, H. Hora and G. Miley, Eds., New York: Plenum Press, 1988, pp. 121–138.

[4] G.E. Sieger, J.H. Yee, and D.J. Mayhall, "Computer Simulation of Nonlinear Coupling of High-Power Microwaves with Slots," IEEE Trans. Plasma Science, vol. 17, pp. 616–621, August 1989.

[5] K.S. Yee, "Numerical Simulation of Initial Boundary Value Problems Involving Maxwell's Equations in Isotropic Media," IEEE Trans. Ant. and Propagat., vol. AP-14, pp. 302-307, 1966.

[6] A.C. Hindmarsh, "Preliminary Documentation of GEARBI: Solution of ODE Systems with Block-Iterative Treatment of the Jacobian," UCID-30149, Lawrence Livermore National Laboratory, Livermore, CA , 1976.